Applied Physics Letters

RESEARCH ARTICLE | JULY 16 2018

Foreshadowing elastic instabilities by negative group velocity in soft composites

Viacheslav Slesarenko; Pavel I. Galich; Jian Li; ... et. al

Check for updates

Appl. Phys. Lett. 113, 031901 (2018)
https://doi.org/10.1063/1.5042077

View Online
Export Citation
CrossMark

Articles You May Be Interested In

Punica granatum fabricated platinum nanoparticles: A therapeutic pill for breast cancer

AIP Conference Proceedings (May 2018)

A Quicker Way to Solve Series-Parallel Circuits

The Physics Teacher (April 2019)

Emil Cohn's electrodynamics of moving bodies

American Journal of Physics (October 1995)



Time to get excited.
Lock-in Amplifiers – from DC to 8.5 GHz



Find out more
Zurich Instruments

AIP Publishing

Downloaded from http://pubs.aip.org/aip/apl/article-pdf/doi/10.1063/1.5042077/14513801/031901_1_online.pdf

Foreshadowing elastic instabilities by negative group velocity in soft composites

Viacheslav Slesarenko,[1,a)] Pavel I. Galich,[1] Jian Li,[1] Nicholas X. Fang,[2] and Stephan Rudykh[3]
[1]*Faculty of Aerospace Engineering, Technion–Israel Institute of Technology, Haifa, Israel*
[2]*Department of Mechanical Engineering, Massachusetts Institute of Technology, Cambridge, Massachusetts 02139, USA*
[3]*Department of Mechanical Engineering, University of Wisconsin–Madison, Madison, Wisconsin 53706, USA*

(Received 29 May 2018; accepted 26 June 2018; published online 16 July 2018)

We reveal the existence of a state in soft composites, characterized by the omni-directional negative group velocity in the vicinity of elastic instability. We show that the appearance of the negative group velocity in layered and fibrous composites foreshadows microscopic loss of the stability. In contrast with classical instability-induced pattern transformations, the transition between states with positive and negative group velocities is not accompanied by geometrical rearrangements and can be triggered by very fine variation of the compressive deformation in stable composites. Finally, we analyze the effect of the geometrical characteristics and elastic moduli of the constituents on the strain range for induced state with negative group velocities. *Published by AIP Publishing*. https://doi.org/10.1063/1.5042077

Expansion of knowledge about wave propagation phenomena is pivotal to various modern applications, such as ultrasound imaging, noise reducing, and waveguiding. Of particular interest is the exploration of the metamaterials, which can exhibit such exotic wave phenomena as negative phase and group[1,2] velocities, mode splitting[3,4] and conversion,[5] frequency filtering and elimination,[6] electromagnetic and acoustic cloaking,[7,8] one-way[9] and other extraordinary subwavelength transmission phenomena.[10] Soft metamaterials have the potential to actively tune wave propagation by external stimuli.[11–15] The intrinsic connection between wave propagation and elastic instabilities[16–18] opens a way to harness instability induced pattern transformation to create various metamaterials with tunable acoustic properties.[19,20] Here, however, we spotlight that drastic change in the acoustic properties can be harnessed to predict the oncoming buckling of soft composites.

In this letter, we reveal the existence of the special reversible state, preceding the onsets of elastic instabilities in soft composite materials. In particular, we show that the group velocities of the transverse or shear S-waves propagating in layered and fibrous composites (FCs) significantly decrease and then become negative (antiparallel to the phase velocity) in the vicinity of the microscopic instability. Moreover, negative group velocity phenomenon, observed near instability, can be induced for any direction of wave propagation. In contrast with instability-induced pattern transformations, the transition between states with positive (PGV) and negative (NGV) group velocities is fully reversible and is not accompanied by any significant changes in the composite geometry. Remarkably, this transition can also be used for achieving extremely low group velocity, also known in literature as slow light[21,22] or sound.[23] This, in turn, can be used to improve the nonlinear wave interactions,[24–26] which can further facilitate design of controllable phase shifters, optical/acoustical amplifiers, and other novel acousto-optical devices.[27]

To analyze S-wave propagation in finitely deformed periodic materials, we consider small amplitude motions superimposed on a finitely deformed state.[17] Recall that in a periodic structure plane waves can be described by the Bloch function.[6] Consequently, we implement the small amplitude motions in terms of Bloch waves $\mathbf{u}(\mathbf{x},t) = \mathbf{U}(\mathbf{x})\exp[i(\mathbf{k}\cdot\mathbf{x} - \omega t)]$, where $\mathbf{u}$ is the incremental displacement, ω is the angular frequency, $\mathbf{k}$ is the Bloch wave vector in the deformed configuration, and $\mathbf{U}$ is a periodic function subjected to the periodicity condition $\mathbf{U}(\mathbf{x}+\mathbf{r}) = \mathbf{U}(\mathbf{x})$ with $\mathbf{r}$ being a spatial periodicity vector in the deformed configuration. To perform the analysis, we utilize the finite element method with the help of COMSOL 5.2a. By gradually increasing the applied deformation, we obtain a solution for the finitely deformed periodic composite. Then, we superimpose the Bloch-Floquet conditions on the deformed state for each strain level. Sweeping through the values of $\mathbf{k}$, we find the corresponding solutions of the eigenvalue problems, associated with the wave equation. Therefore, for each level of deformation, we obtain the dispersion relation $\omega(\mathbf{k})$ vs $\mathbf{k}$. The deformation level, for which $\omega(\mathbf{k}) = 0$ ($\mathbf{k} \neq \mathbf{0}$) appears, corresponds to the onset of elastic instabilities. For detailed description of this procedure, readers are referred to the previous works employing this method.[18,28]

We describe the behavior of composite constituents with the neo-Hookean strain energy density function integrated in COMSOL 5.2a as

$$\psi = \frac{\mu}{2}(\mathbf{F}:\mathbf{F}-3) - \mu\ln(\det\mathbf{F}) + \frac{\Lambda}{2}(\ln(\det\mathbf{F}))^2, \quad (1)$$

where $\mathbf{F}$ is the deformation gradient within the composite constituent, μ is the shear modulus, and Λ is the first Lame's parameter; recall that Λ relates to the bulk modulus as

a)Electronic addresses: slslesarenko@technion.ac.il and sl.slesarenko@gmail.com

Downloaded from http://pubs.aip.org/aip/apl/article-pdf/doi/10.1063/1.5042077/14513801/031901_1_online.pdf

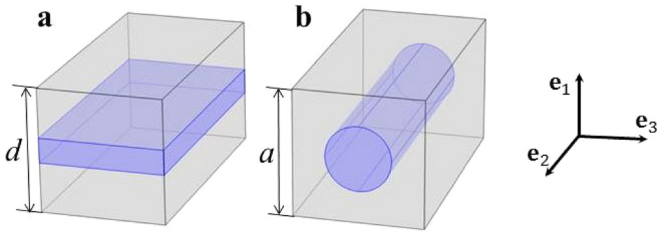


FIG. 1. RVEs of layered (a) and fibrous (b) composites.

$K = \Lambda + 2\,\mu/3$. The double dot product $\mathbf{F} : \mathbf{F}$ reads as $\mathbf{F} : \mathbf{F} = \mathrm{F}_{ij}\mathrm{F}_{ij}$ in index notation. To preserve the nearly incompressible behavior of the constituents, we set a high ratio between the first Lame's parameter and the shear modulus, namely, $\Lambda/\mu = 10^3$ in all simulations. Figure 1 presents the representative volume elements (RVEs) for the layered composites (LCs) and fibrous composites (FCs) considered in this work. For completeness, we verified our numerical results against the exact analytical solutions for finitely deformed 3D periodic layered[12] and fibrous[15] materials in the long wave limit, and found an excellent agreement.

In the central part of this letter, we consider a periodic layered composite constructed of two alternating phases with the volume fractions v_l and $v_m = 1 - v_l$, subjected to in-plane deformation defined by the following homogeneous macroscopic deformation gradient:

$$\bar{\mathbf{F}}_{ps} = \lambda^{-1}\mathbf{e}_1 \otimes \mathbf{e}_1 + \lambda\mathbf{e}_2 \otimes \mathbf{e}_2 + \mathbf{e}_3 \otimes \mathbf{e}_3, \tag{2}$$

where λ is the applied macroscopic stretch ratio, $\otimes$ denotes tensor product, and the basis vectors are specified in Fig. 1. The similar analysis for layered and fibrous composites subjected to uniaxial compression in a fully 3D framework is presented in the supplementary material. Here and thereafter, the fields and parameters of the constituents are denoted by subscripts $(\bullet)_l$ and $(\bullet)_m$. Geometrically, the layers are characterized by their thicknesses $d_l = v_l d$ and $d_m = v_m d$, where d is the initial period of the laminate [see Fig. 1(a)].

Recall that the soft composites with periodic microstructure, such as LCs or FCs, may lose their stability under deformation. In general, the elastic instabilities are associated with the loss of ellipticity of the equilibrium equations. Depending on the period of the newly formed buckled shape, the instabilities can be classified as macroscopic or microscopic.[16,29,30] Macroscopic instabilities are characterized by the critical wavelength, significantly exceeding the period of the structure, while microscopic loss of the stability is associated with the formation of a new periodicity, comparable with the dimensions of the primitive unit cell.[28,31,32]

We start with the wave propagation analysis in LCs undergoing instabilities via the macroscopic mechanism. Here, we focus on S-waves propagating in the direction of the layers with wavevector $\mathbf{k} = k_2\mathbf{e}_2$ and in-plane polarization along $\mathbf{e}_1$ vector, because their phase velocities become zero first upon achieving critical deformation.[12] Figure 2 shows the frequency (a), the phase velocity (b), and the group velocity (c) as functions of the normalized wavenumber $\tilde{k}_2 = k_2 d/(2\pi)$ for the in-plane S-wave propagating along the layers in the LC with $v_l = 0.2$ and $\mu_l/\mu_m = 15$ subjected to the in-plane contractions (2) along the layers. The frequency is normalized as $f^* = \frac{\omega d}{2\pi}\sqrt{\bar{\rho}/\bar{\mu}}$, and the phase and group velocities are normalized by $\mathrm{v}_0 = \sqrt{\bar{\mu}/\bar{\rho}}$, where $\bar{\mu} = (v_l/\mu_f + v_m/\mu_m)^{-1}$ is the weighted harmonic mean shear modulus and $\bar{\rho} = v_l\rho_l + v_m\rho_m$ is the weighted arithmetic mean phase density. Here and thereafter, we consider composites with constituents having identical densities, namely, $\rho_l/\rho_m = 1$. Clearly, the contraction of the LC along the layers, especially for stretches approaching to the critical value $\lambda_{cr}^{macro} = 0.906$, considerably influences the long S-waves. In particular, the phase velocities of the long S-waves significantly decrease in the contracted LC [see Fig. 2(b)]. Finally, when the applied stretch reaches the critical value, the phase velocity for $\tilde{k}_2 \to 0$ becomes zero, which corresponds to the macroscopic loss of stability. However, the contraction barely influences phase velocities of the short S-waves with the wavelengths being slightly lower than the period of the LC ($l \lesssim d$, where $l = 2\pi/k_2$ denotes wavelength). The group velocities of S-waves in the contracted LC can either increase or decrease depending on the wavelength, but for all stretches they remain positive [see Fig. 2(c)].

Remarkably, the picture is completely different for the in-plane S-wave in the LCs undergoing instabilities via the microscopic mechanism. Figure 3 shows the frequency (a), the phase velocity (b), and the group velocity (c) as functions

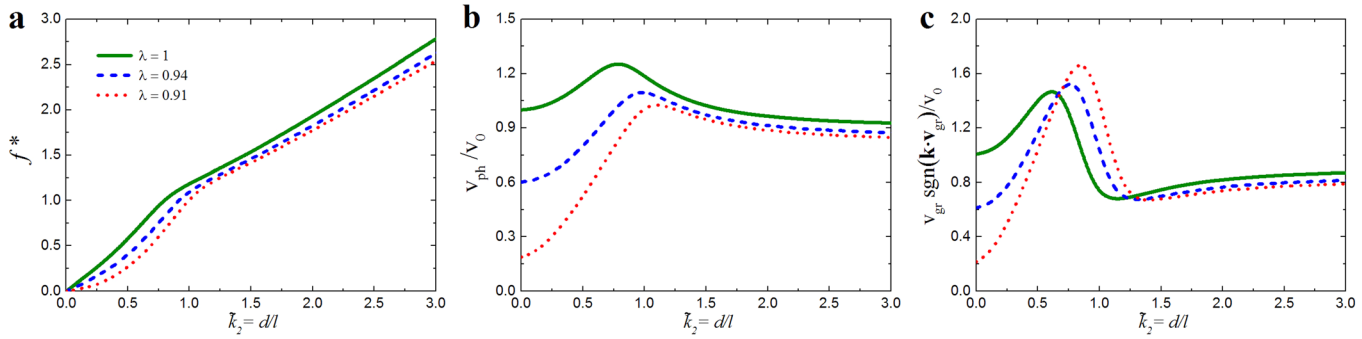


FIG. 2. Frequency (a), phase velocity (b), and group velocity (c) curves against wavenumber for the in-plane S-waves propagating along the layers in LC with $v_l = 0.2$, $\mu_l/\mu_m = 15$, and $\rho_l/\rho_m = 1$. The LC is subjected to the in-plane contractions of $\lambda = 0.91$ (dotted red curves), $\lambda = 0.94$ (dashed blue curves), and $\lambda = 1$ (continuous green curves). The corresponding critical stretch ratio is $\lambda_{cr}^{macro} = 0.906$. The frequency is normalized as $f^* = \frac{\omega d}{2\pi}\sqrt{\bar{\rho}/\bar{\mu}}$; velocities are normalized by $\mathrm{v}_0 = \sqrt{\bar{\mu}/\bar{\rho}}$.

Downloaded from http://pubs.aip.org/aip/apl/article-pdf/doi/10.1063/1.5042077/14513801/031901_1_online.pdf

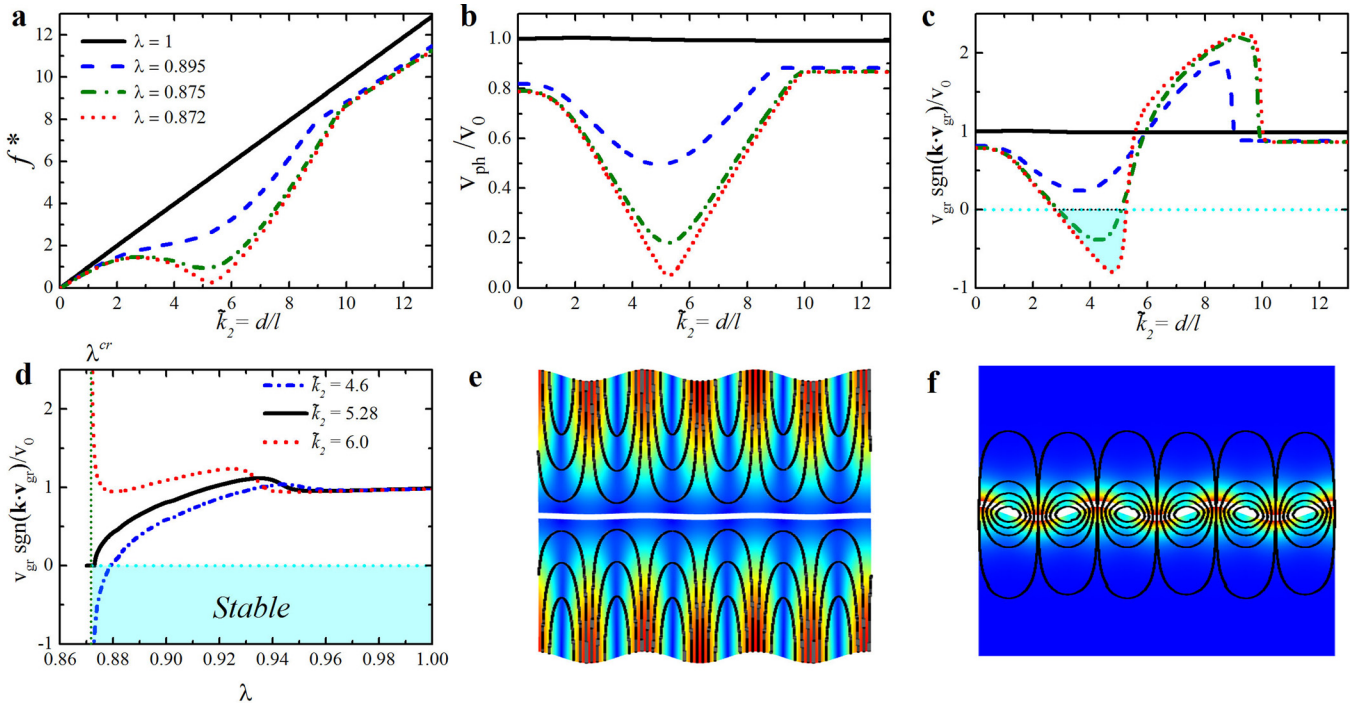


FIG. 3. Frequency (a), phase velocity (b), and group velocity (c) curves vs normalized wavenumber ($\tilde{k}_2$) for the waves propagating along the layers in the layered composite (LC) with $v_f = 0.02$ and $\mu_l/\mu_m = 15$. The LC is subjected to the in-plane contractions of $\lambda = 0.872$ (dotted red curves), $\lambda = 0.875$ (dashed-dotted green curves), $\lambda = 0.895$ (dashed blue curves), and $\lambda = 1$ (continuous black curves). Dependence of group velocity on stretch ratio λ (d) and eigenmodes ($\tilde{k}_2 = 4.6$) for undeformed ($\lambda = 1$) (e) and deformed ($\lambda = 0.873$) (f) LC. The area filled in blue color corresponds to the negative group velocity (NGV) region (c) and (d). The color on the eigenmodes shows the relative displacement amplitude (blue—lowest, red—highest); the black streamlines represent the displacement direction tangents (e) and (f).

of the normalized wavenumber for the in-plane S-wave propagating along the layers in the LC with $v_l = 0.02$ and $\mu_l/\mu_m = 15$ subjected to the in-plane contractions (2) along the layers. Note that the LC loses the elastic stability at critical stretch ratio $\lambda^{cr} = 0.871$ with the corresponding wavelength of $l^{cr} = 0.19d$. Now, the contraction of the LC, especially for stretches approaching to the critical value, preferably affects the S-waves with the wavelength being lower than the period of LC, namely, $d/10 \lesssim l \lesssim d$. In particular, the dispersion curves develop negative slopes [see Fig. 3(a)], resulting in the appearance of negative group velocity induced by compressive deformation in yet stable composite [Fig. 3(c)]. Figure 3(d) shows evolution of group velocities as functions of applied deformation at different normalized wavenumbers $\tilde{k}_2$. Initially, applied deformation results just in slight linear changes in the group velocity values. However, after reaching a certain compressive deformation level, the dependence becomes highly non-linear. Note that $\tilde{k}_2 = \tilde{k}_2^{cr} = 5.28$ corresponds to the critical wavenumber, which defines the new postbuckling structure to be developed upon exceeding the critical level of compressive deformation. We note that negative group velocity cannot be induced in the stable composite for $\tilde{k}_2 \geq \tilde{k}_2^{cr}$ [see Fig. 3(d)]; whereas, for $\tilde{k}_2 < \tilde{k}_2^{cr}$, NGV can be induced by deformation. Note that the material remains stable in the observed NGV state until critical stretch value is reached. Remarkably, the similar behavior is observed in the fibrous and layered composites subjected to the uniaxial compression in a fully 3D framework (see the supplementary material for details). Therefore, when the primary buckling mode of the LCs or FCs corresponds to the microscopic instability, the negative group velocity for the S-waves, propagating along the layer/fiber direction, is observed in the vicinity of the critical stretch.

Figures 3(e) and 3(f) illustrate the deformation induced change in the wave propagation modes; the modes are plotted for the undeformed [$\lambda = 1$ shown in Fig. 3(e)] and deformed [$\lambda = 0.873$ shown in Fig. 3(f)] states. In the undeformed state, the maximal displacement amplitude occurs in the soft matrix, whereas, in the deformed LC, the largest part of the energy propagates through the stiff layer, where the maximal displacement amplitude is observed [see Fig. 3(f)]. We should note that this switch in the wave modes occurs at the compressive deformation level ($\lambda \approx 0.94$ for $\tilde{k}_2 = 4.6$), which corresponds to the change in the dependence of group velocity on compressive deformation [see Fig. 3(d)]; a further increase in the compressive level leads to a rapid decrease in the group velocity value, which then changes the sign and becomes negative (if $\tilde{k}$ lies in the NGV admissible wavenumber range).

Thus far, we analyzed the S-waves propagating in the direction of layers only. To clarify how the characteristics of in-plane S-wave change with the propagation direction, we present the equi-frequency contours in Fig. 4. We observe the negative group velocity in the vicinity of the microscopic instability for all directions of wave propagation with the only exception of direction perpendicular to the layers. The region of wavevectors for which group velocity is antiparallel to phase velocity is bounded by dashed red lines in Fig. 4. Note that in contrast with classical 2D-phononic crystals, where the equi-frequency contours are closed curves, for LC the equi-frequency contours in the vicinity of the elastic instability are the straight open lines due to the absence of crystal periodicity in the layer direction. Based on Fig. 4, we

Downloaded from http://pubs.aip.org/aip/apl/article-pdf/doi/10.1063/1.5042077/14513801/031901_1_online.pdf

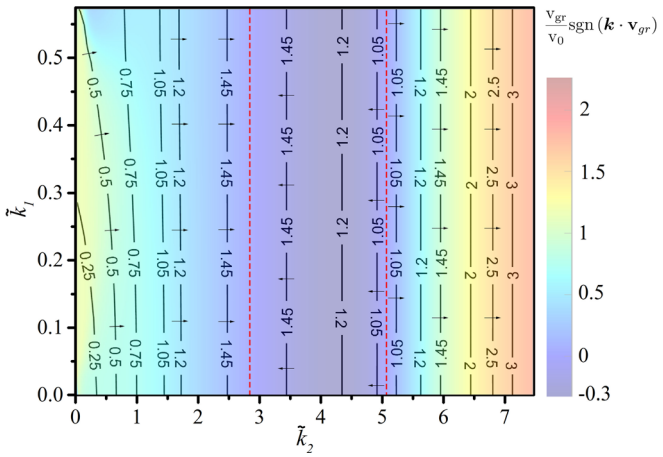


FIG. 4. Equi-frequency contours in the LC with $v_f = 0.02$ and $\mu_f/\mu_m = 15$ subjected to in-plane contraction with $\lambda = 0.875$. The color represents an absolute value of the group velocity and its direction with respect to the phase velocity. The arrows denote the direction of the group velocity. The region bounded by dashed red lines corresponds to the region with negative group velocity.

can also conclude that the frequency range, for which the negative group velocity ($\boldsymbol{k}\cdot\mathbf{v}_{gr} < 0$) is observed, is independent of the wave propagation direction.

We revealed that in LCs (and also 3D periodic fiber composites discussed in the supplementary material) NGV state precedes the onset of the microscopic instability. A question, however, arises: how wide is the range of deformations, where NGV behavior is observed in stable composites? Figure 5 shows the width of the corresponding stretch range $\Delta\lambda$ (in percent) for the NGV state as the function of stiffer layer volume fraction and contrast in elastic moduli. The $\Delta\lambda$ width is calculated as the difference between the stretch λ_0 for which the negative slope of the dispersion curve is first identified and the critical stretch λ^{cr}. It appears that $\Delta\lambda$ tends to increase with a decrease in the elastic modulus contrast and the volume fraction of stiffer layers. For instance, for the LC with $v_l = 0.1$ and $\mu_l/\mu_m = 25$ (the onset of instability at $\lambda^{cr} = 0.912$ and at the wavelength of $l^{cr} = 1.30d$), the width of the NGV state is only 0.14%, while for the composite with $v_l = 0.01$ and $\mu_l/\mu_m = 5$ it is 1.5%. The dashed curve in Fig. 5 separates the compositions

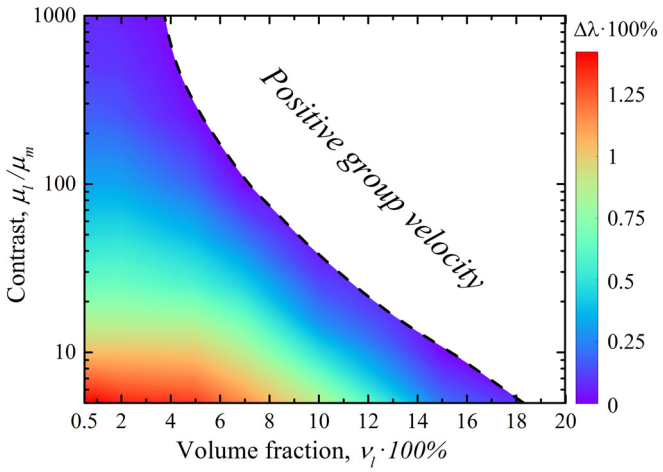


FIG. 5. The NGV strain level width for stable LCs with various volume fractions and shear modulus contrasts. The width of the region with negative group velocity is calculated as $(\lambda_0 - \lambda^{cr})\cdot 100\%$.

of the LCs, in which the revealed NGV state precedes the elastic instability, from the compositions corresponding to the composites, in which the group velocity of S-waves, propagating along the layers, remains positive until the buckling. At the same time, due to the existing intrinsic connection between NGV state and elastic instabilities, the same dashed curve separates the LCs that undergo microscopic instabilities (with compositions laying on the left side), from those, that experience macroscopic loss of stability (with compositions laying on the right side). We note that we have found similar behavior in LCs and 3D periodic fiber composite subjected to uniaxial compression in fully 3D settings.

We revealed the dramatic changes in the characteristics of the S-waves propagating in finitely deformed layered and fibrous materials prior to the stability loss. In particular, we demonstrated that there is a special state in layered and fibrous composites in the vicinity of the elastic instability, which is characterized by the omni-directional negative group velocities. Thus, the appearance of NGV state foreshadows the onset of microscopic instability. Moreover, since the composites remain stable in the vicinity of the instability point, the transition between the states with positive and negative group velocities is reversible and can be triggered by small controllable variation of the compressive deformation. The strain range for which the group and phase velocities are antiparallel ($\boldsymbol{k}\cdot\mathbf{v}_{gr} < 0$) is relatively narrow; however, it can be increased by decreasing the elastic modulus contrast and the volume fraction of the stiffer layers. Finally, we note that since the finite deformation of the soft materials can be induced by other external stimuli,[33–35] potentially the observed NGV state can be induced and controlled, for instance, by external electric field.[36,37]

See supplementary material for the similar analysis of S-wave propagation near elastic instabilities in fibrous and layered composites subjected to compression in 3D formulation.

This research was supported by Grant No. 2016284 from the United States-Israel Binational Science Foundation (BSF). V.S. is thankful for the support through the Technion Postdoctoral Fellowship. P.G. is thankful for the support through the Jacobs Fellowship. J.L. gratefully acknowledges the support through the Lady Davis Fellowship.

[1]S. H. Lee, C. M. Park, Y. M. Seo, Z. G. Wang, and C. K. Kim, Phys. Rev. Lett. **104**, 054301 (2010).
[2]N. Fang, D. Xi, J. Xu, M. Ambati, W. Srituravanich, C. Sun, and X. Zhang, Nat. Mater. **5**, 452 (2006).
[3]Z. Chang, H.-Y. Guo, B. Li, and X.-Q. Feng, Appl. Phys. Lett. **106**, 161903 (2015).
[4]P. I. Galich and S. Rudykh, Appl. Phys. Lett. **107**, 056101 (2015).
[5]J.-H. Sun and T.-T. Wu, Phys. Rev. B **74**, 174305 (2006).
[6]M. Kushwaha, P. Halevi, L. Dobrzynski, and B. Djafari-Rouhani, Phys. Rev. Lett. **71**, 2022 (1993).
[7]D. Schurig, J. J. Mock, B. J. Justice, S. A. Cummer, J. B. Pendry, A. F. Starr, and D. R. Smith, Science **314**, 977 (2006).
[8]S. Zhang, C. Xia, and N. Fang, Phys. Rev. Lett. **106**, 024301 (2011).
[9]X.-F. Li, X. Ni, L. Feng, M.-H. Lu, C. He, and Y.-F. Chen, Phys. Rev. Lett. **106**, 084301 (2011).
[10]J. Christensen, L. Martin-Moreno, and F. J. Garcia-Vidal, Phys. Rev. Lett. **101**, 014301 (2008).

Downloaded from http://pubs.aip.org/aip/apl/article-pdf/doi/10.1063/1.5042077/14513801/031901_1_online.pdf

[11]W. J. Parnell, A. N. Norris, and T. Shearer, Appl. Phys. Lett. **100**, 171907 (2012).
[12]P. I. Galich, N. X. Fang, M. C. Boyce, and S. Rudykh, J. Mech. Phys. Solids **98**, 390 (2017).
[13]M. Gei, S. Roccabianca, and M. Bacca, IEEE/ASME Trans. Mechatronics **16**, 102 (2011).
[14]M. Destrade and R. W. Ogden, Math. Mech. Solids **16**, 594 (2011).
[15]P. I. Galich, V. Slesarenko, and S. Rudykh, Int. J. Solids Struct. **110–111**, 294 (2017).
[16]G. Geymonat, S. Müller, and N. Triantafyllidis, Arch. Ration. Mech. Anal. **122**, 231 (1993).
[17]K. Bertoldi and M. C. Boyce, Phys. Rev. B **78**, 184107 (2008).
[18]P. I. Galich, V. Slesarenko, J. Li, and S. Rudykh, Int. J. Eng. Sci. **130**, 51 (2018).
[19]P. Wang, F. Casadei, S. Shan, J. C. Weaver, and K. Bertoldi, Phys. Rev. Lett. **113**, 014301 (2014).
[20]Y. Chen, T. Li, F. Scarpa, and L. Wang, Phys. Rev. Appl. **7**, 024012 (2017).
[21]T. Baba, Nat. Photonics. **2**, 465 (2008), 0504112.
[22]J. G. Pedersen, S. Xiao, and N. A. Mortensen, Phys. Rev. B **78**, 153101 (2008).
[23]W. M. Robertson, C. Baker, and C. B. Bennett, Am. J. Phys. **72**, 255 (2004).
[24]K. Sakoda, Opt. Express **4**, 167 (1999).
[25]C. Monat, M. de Sterke, and B. J. Eggleton, J. Opt. **12**, 104003 (2010).
[26]R. P. Moiseyenko and V. Laude, Phys. Rev. B **83**, 064301 (2011).
[27]A. H. Safavi-Naeini, T. P. M. Alegre, J. Chan, M. Eichenfield, M. Winger, Q. Lin, J. T. Hill, D. E. Chang, and O. Painter, Nature **472**, 69 (2011).
[28]V. Slesarenko and S. Rudykh, J. Mech. Phys. Solids **99**, 471 (2017).
[29]N. Triantafyllidis and W. C. Schnaidt, J. Mech. Phys. Solids **41**, 1533 (1993).
[30]J. C. Michel, O. Lopez-Pamies, P. Ponte Castaeda, and N. Triantafyllidis, J. Mech. Phys. Solids **58**, 1776 (2010).
[31]N. Triantafyllidis and B. N. Maker, J. Appl. Mech., Trans. ASME **52**, 794 (1985).
[32]J. Li, V. Slesarenko, P. I. Galich, and S. Rudykh, Composites Part B **148**, 114 (2018).
[33]R. Pelrine, R. Kornbluh, Q. Pei, and J. Joseph, Science **287**, 836 (2000).
[34]G. Y. Zhou and Z. Y. Jiang, Smart Mater. Struct. **13**, 309 (2004).
[35]J. Huang, T. Li, C. Chiang Foo, J. Zhu, D. R. Clarke, and Z. Suo, Appl. Phys. Lett. **100**, 041911 (2012).
[36]P. I. Galich and S. Rudykh, J. Appl. Mech. **84**, 091002 (2017).
[37]M. Jandron and D. L. Henann, Int. J. Solid Struct. (published online 2018).

Downloaded from http://pubs.aip.org/aip/apl/article-pdf/doi/10.1063/1.5042077/14513801/031901_1_online.pdf